Dual-Band GaN MMIC Power Amplifier for Microwave Backhaul Applications

Dual-band GaN MMIC Power Amplifier for Microwave Backhaul applications

Roberto Quaglia *Member, IEEE*, Vittorio Camarchia *Senior Member, IEEE*, Marco Pirola *Member, IEEE*

***Abstract*—Design and characterization of a dual-band (7 GHz and 15 GHz) MMIC GaN linear Power Amplifier are presented. The amplifier, suitable for point-to-point microwave backhaul applications, exploits a TriQuint GaN foundry process. Large signal measurements exhibit power gain higher than 10 dB and 7 dB in the lower and higher bands respectively, and saturated output power of 34.7 dBm, in a 15 % band around the two center frequencies.**

***Index Terms*—Backhaul networks, monolithic microwave integrated circuit (MMIC), dual-band, Gallium Nitride (GaN).**

I. Introduction

MICROWAVE backhaul infrastructure needs to evolve to satisfy the high requirements in terms of data rates of 3/4G applications like Long Term Evolution (LTE) or WiMAX. From the Power Amplifier (PA) standpoint, this means either to adapt the present technologies and architectures to the new scenario, mainly by increasing the working frequency [1], and/or to refer to new technologies and strategies. Recently, some GaN based examples outperforming the corresponding GaAs counterparts have been presented [2]–[5], demonstrating the potentialities of this technology. However, all those examples are limited to the lower backhaul licensed band (7 GHz), and focused on the performance optimization on a single frequency band.

In this framework, we present a GaN Microwave Monolithic Integrated Circuit (MMIC) dual-band PA working at 7 and 15 GHz where it exhibits interesting power performances, together with satisfactory linearity behavior.

Dual-band PAs are well established in literature, with several hybrid examples available (see e.g.[6], [7]) and impressive performances for frequencies however below few GHz. Higher frequency examples resort to CMOS technology exhibiting limited output power and efficiency [8], [9].

Concurrent use of a dual-band PA for microwave backhauls is presently not interesting. However, availability of multi-band PAs ensuring back-compatibility with the systems in use (antennas, duplexers, cables, ecc.) and, at the same time, working at higher frequency where more band is available, represents a very attractive scenario.

II. Design

TriQuint Semiconductor GaN foundry has been adopted for design development and realization. The monolithic process is based on 0.25 μm HEMT AlGaN/GaN on SiC supplying a power density around 4.5 W/mm at 7 GHz with drain bias of 30 V. Given the required 4 W saturated output power, accounting for estimated output network losses, and considering the model availability in the foundry design kit, the selected PA configuration has been a combined stage adopting two 8×75 μm devices. According to a class AB design strategy, a drain bias current of around 10% of I_{DSS} has been adopted.

Three constitutive blocks can be identified in the amplifier structure: output matching network, input power splitter, and input matching networks. In a first phase the three blocks have been designed separately adopting simplified equivalent circuits for the non-linear device. Final overall extensive optimizations have been then carried out adopting non-linear simulations with the foundry models.

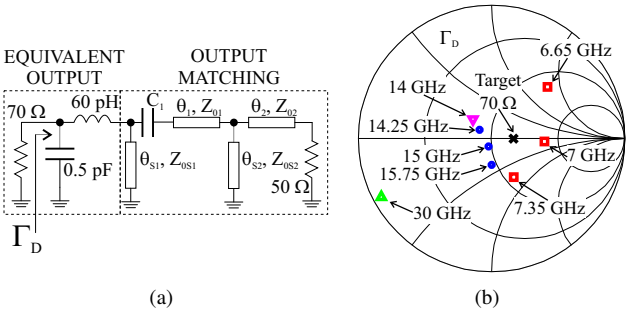

(a) (b)

Fig. 1. Block scheme of the output matching design strategy (a) and simulated Γ_{D} (b).

Concerning the design of the output matching circuit, load-pull simulations on the combined device pair have been performed to identify the optimum load for maximum power in the two bands of interest (around 7 and 15 GHz). Regarding second harmonic, for the 15 GHz band a tuned load approach has been followed, while for the 7 GHz band, due to the frequency overlap with the higher band, a short circuit termination was not achievable. Thus, the effects of complex second harmonic load have been verified *a posteriori* through non-linear simulations, to assess its impact on power performances with respect to a tuned load case. The equivalent circuit reported in Fig. 1(a) has been then extracted and used to design the matching network in a CAD linear simulation environment. The matching network adopted topology is sketched in Fig. 1(a): the first stub and the capacitor C_1 provide bias-tee functions too. The lengths and impedances of the different lines maximize the power transfer from the 70 Ω port (real optimum load of the combined devices) to the 50 Ω port in the two frequency bands. Satisfactory matching results, on

R. Quaglia, V. Camarchia and M. Pirola are with the Department of Electronics and Telecommunications, Politecnico di Torino, C.so Duca degli Abruzzi 24, 10129 Torino, ITALY e-mail: vittorio.camarchia@polito.it

V. Camarchia is also with the Center for Space Human Robotics, Italian Institute of Technology, C.so Trento 21, 10129 Torino, ITALY

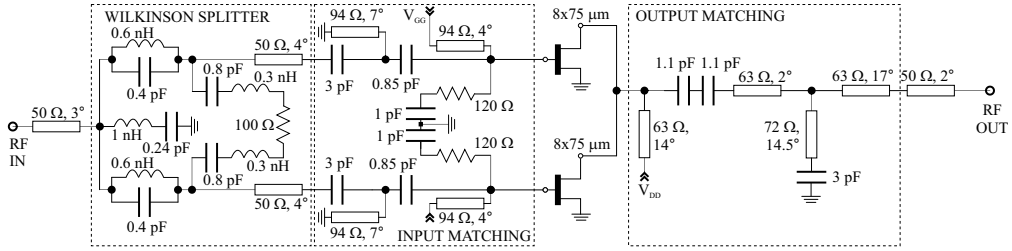

Fig. 2. Complete scheme of the DBPA. Equivalent ideal lines are represented: electrical length refer to 7 GHz.

both bands, have been achieved. The synthesized loads at the intrinsic plane Γ_D are reported in Fig. 1(b) for the two bands and their harmonics, and they have been obtained adopting the component values indicated in Fig. 2.

Concerning the PA input section, as already outlined, matching and power splitting designs have been decoupled, matching both blocks at 50 Ω. Adopting this strategy, a 50 Ω Wilkinson divider has been chosen for input power splitting. Its layout has been optimized for compactness, emphasizing symmetry to avoid odd mode excitation. A lumped approach has been pursued using MIM capacitors and inductors, according to the design guidelines suggested in [10].

Active device input impedance, derived through large signal simulations at both operative frequency, has been modeled with an R-C series as shown in Fig. 3(a). Using this representation, input matching network has been realized with a Π-network (see Fig. 3(a)). In fact, adopting $L_1 = 270$ pH, $C_2 = 1$ pF and $L_3 = 160$ pH, a good matching has been achieved in the two frequency bands. In the final layout, inductors have been replaced by high-impedance short-ended stubs (L_3 also provides the gate bias V_{GG}). Fig. 3(b) shows the S_{11} for the circuit of Fig. 3(a).

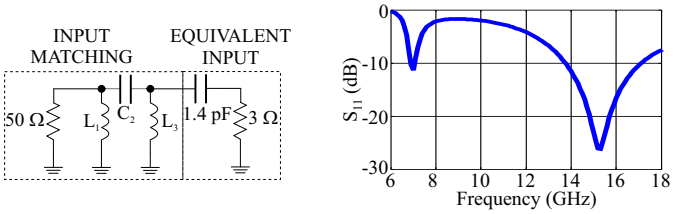

Fig. 3. Block scheme of the input matching design strategy (a) and simulated reflection coefficient at the 50 Ω port (b).

Effects of MMIC process variability have been comprehensively appraised through Monte Carlo analysis. Given the resonant nature of the dual band structures, it has not been possible to obtain a wideband behaviour ensuring a low process sensitivity in both bands. As a result, in the upper band, where we managed to ensure a rather wideband behaviour, process variations are expected not to sensibly shift the center frequency of operation. In fact, at 15 GHz, the standard deviation of the magnitude of S_{21} is around 4%. At 7 GHz, this value is instead of 16% and, as a consequence, higher deviations of the MMIC behavior with respect to the nominal design are expected.

The effect of the 7 GHz band second harmonic, according to non-linear simulations, resulted negligible, maintaining similar performances to a tuned load case in terms of efficiency and output power.

The complete scheme of the amplifier is reported in Fig. 2, where all the component values are indicated. The input matching network includes a R-C series stabilization network, designed and optimized by means of loop stability analysis to ensure broadband stability. Fig. 4 shows a microscope picture of the MMIC: the size is $2.7 \times 1.5\,\text{mm}^2$. The constitutive blocks of the PA are marked on the picture.

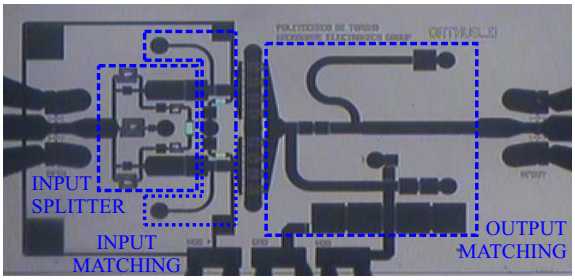

Fig. 4. A microscope picture of the fabricated dual-band PA. Chip size: $2.7 \times 1.5\,\text{mm}^2$.

III. Experimental Characterization

The fabricated MMICs have been characterized in small and large signal Continuous Wave (CW) conditions by using a real-time power measurement bench [11] for a Class AB bias point of $I_D = 80$ mA, $V_{DS} = 30$ V. Scattering measurements have been performed in the 6-18 GHz frequency range. In a 15% frequency band around 7 GHz (15 GHz) the PA evidenced a small signal gain around 10 dB (7 dB), together with return loss always better than 10 dB (7 dB). The lower band exhibits a more marked frequency shift (gain peak at 7.7 GHz) than the higher one (gain peak at 15.5 GHz), see Fig. 5. Efficiency, power added efficiency (PAE), power gain and AM/PM distortion as a function of the output power are shown in Fig. 6. This figure is relative to 7.7 and 14.9 GHz frequencies for the measured results, where the MMIC yields its best power performances. Frequency shifts affect also large signal performances, reducing the saturated power, that however, in both bands, exceeds 34.6 dBm. The efficiency (PAE) results higher than 32% (24%) and 37% (29%) at 7.7 GHz and 14.9 GHz, respectively. The comparison with simulations shows that the frequency shift in the lower band also affected the power performances. Moreover, a gain compression higher than expected emphases the PAE degradation at saturation. In the upper band,

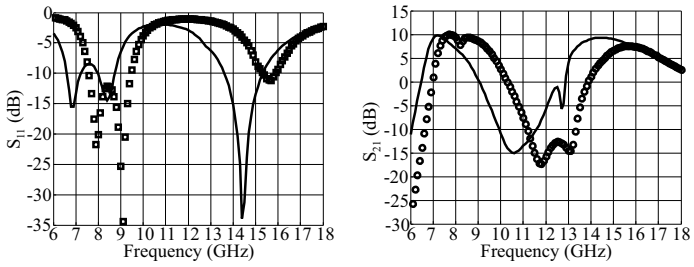

Fig. 5. Scattering parameters in the range 6-18 GHz. S_{11} (a), S_{21} (b). Measured: symbols, simulated: solid lines. Bias: $I_{\mathrm{D}} = 80$ mA, $V_{\mathrm{DS}} = 30$ V.

the measurements are more in agreement with simulations. Regarding linearity, Fig. 6(d) shows promising results in terms

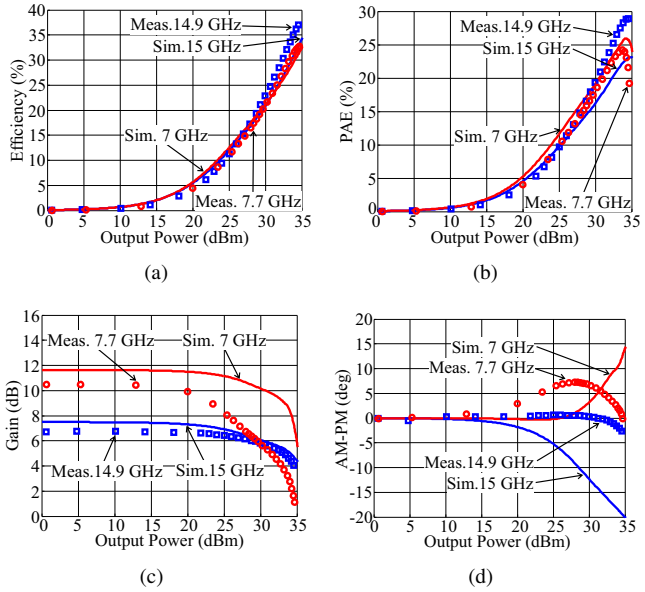

Fig. 6. CW results at lower (red) and upper (blue) band.Simulated: solid lines, measured: symbols. Bias: $I_{\mathrm{D}} = 80$ mA, $V_{\mathrm{DS}} = 30$ V.

of measured AM/PM, since digital predistortion can handle up to 3/4 dB of AM/AM distortion, while more critical issues concern AM/PM. In fact, a limited phase distortion, as the one here obtained, is really welcomed by equipment suppliers and end-users [12]. The non-linear simulations are in this case not in agreement with the measured results, since the non/linear model is not able to predict with the required accuracy the phase distortion.

Concerning the power behavior vs. frequency, output power, gain and efficiency are shown in Fig. 7, where both simulations and measurements are reported. The peak power is 34.7 dBm, with 1 dB and 1.5 dB ripple in the 7.8-8.2 GHz, and 14-16 GHz bands, respectively. Efficiency in the lower band is satisfactory around 7.7 GHz, then, due to the experienced frequency shift, it rapidly decreases. The gain vs. frequency is relatively flat around 10 dB. In the higher band, the frequency shift of measurements with respect to simulations is less noticeable, and best gain/efficiency performances are measured around 15 GHz. If compared to other GaN MMIC examples at 7 GHz [5], the present PA shows inferior performance at single frequency, but is able to guarantee dual band operation.

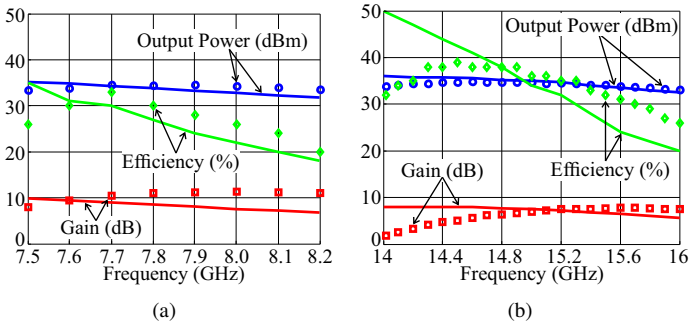

Fig. 7. Single tone CW characterization in the two designed bands. Output power (blue), gain (red) and efficiency (green). Simulations: solid lines, measurements: symbols. Bias: $I_{\mathrm{D}} = 80$ mA, $V_{\mathrm{DS}} = 30$ V.

IV. Conclusion

The paper demonstrates the feasibility of a dual band GaN MMIC PA for backhaul applications. The key design steps have been described. Promising results, in terms of output power and efficiency, have been found in both bands, suggesting possible employment of this technology/architecture in multi-band backhaul applications.

References

[1] S. Chia, M. Gasparroni, and P. Brick, "The next challenge for cellular networks: backhaul," *IEEE Microw. Mag.*, vol. 10, no. 5, pp. 54 –66, Aug. 2009.

[2] D. Gustafsson, J. C. Cahuana, D. Kuylenstierna, I. Angelov, N. Rorsman, and C. Fager, "A Wideband and Compact GaN MMIC Doherty Amplifier for Microwave Link Applications," *IEEE Trans. Microw. Theory Tech.*, vol. 61, no. 2, pp. 922 –930, Feb. 2013.

[3] V. Camarchia, J. Fang, J. Moreno Rubio, M. Pirola, and R. Quaglia, "7 GHz MMIC GaN Doherty Power Amplifier with 47% efficiency at 7 dB output back-off," *IEEE Microw. Wireless Compon. Lett.*, vol. 23, no. 1, pp. 34–36, Jan. 2013.

[4] L. Piazzon, P. Colantonio, F. Giannini, and R. Giofrè, "15% Bandwidth 7 GHz GaN-MMIC Doherty Amplifier With Enhanced Auxiliary Chain," *Microwave and Optical Technology Letters*, vol. 56, no. 2, pp. 502–504, Feb. 2014.

[5] V. Camarchia, J. Moreno Rubio, M. Pirola, R. Quaglia, P. Colantonio, F. Giannini, R. Giofre, L. Piazzon, T. Emanuelsson, and T. Wegeland, "High-Efficiency 7 GHz Doherty GaN MMIC Power Amplifiers for Microwave Backhaul Radio Links," *IEEE Trans. Electron Devices*, vol. 60, no. 10, pp. 3592–3595, 2013.

[6] P. Colantonio, F. Giannini, R. Giofrè, and L. Piazzon, "Simultaneous dual-band high efficiency harmonic tuned power amplifier in GaN technology," in *Microwave Integrated Circuit Conference, 2007. EuMIC 2007. European*, 2007, pp. 127–130.

[7] P. Saad, P. Colantonio, L. Piazzon, F. Giannini, K. Andersson, and C. Fager, "Design of a Concurrent Dual-Band 1.8–2.4-GHz GaN-HEMT Doherty Power Amplifier," *IEEE Trans. Microw. Theory Tech.*, vol. 60, no. 6, pp. 1840–1849, 2012.

[8] Y.-S. Noh and C.-S. Park, "PCS/W-CDMA dual-band MMIC power amplifier with a newly proposed linearizing bias circuit," *IEEE J. Solid-State Circuits*, vol. 37, no. 9, pp. 1096–1099, 2002.

[9] K.-A. Hsieh, H.-S. Wu, K.-H. Tsai, and C.-K. Tzuang, "A Dual-Band 10/24-GHz Amplifier Design Incorporating Dual-Frequency Complex Load Matching," *IEEE Trans. Microw. Theory Tech.*, vol. 60, no. 6, pp. 1649–1657, 2012.

[10] T. Kawai, I. Ohta, and A. Enokihara, "Design method of lumped-element dual-band wilkinson power dividers based on frequency transformation," in *Microwave Conference Proceedings (APMC), 2010 Asia-Pacific*, 2010, pp. 710–713.

[11] V. Camarchia, V. Teppati, S. Corbellini, and M. Pirola, "Microwave Measurements -Part II Non-linear Measurements," *IEEE Instrum. Meas. Mag.*, vol. 10, no. 3, pp. 34 –39, Jun. 2007.

[12] J. Staudinger, "Effects on AM/AM and AM/PM distortion on spectral regrowth in 3GPP W-CDMA BS power amplification," *Microwave Journal*, vol. 45, no. 11, pp. 90 –97, Nov. 2002.